

NUMERICAL INVESTIGATIONS OF THE AERODYNAMICS AND HANDLING QUALITIES OF A HELICOPTER FLYING ACROSS A WIND TURBINE WAKE

Antonio Visingardi, a.visingardi@cira.it, CIRA (Italy)

Marilena D. Pavel, m.d.pavel@tudelft.nl, Delft University of Technology (The Netherlands)

Abstract

The present paper illustrates the outcomes of a research activity carried out by CIRA and the Delft University of Technology in the framework of the GARTEUR HC/AG-23 action group. This activity has been aimed at investigating, from the aerodynamic and handling qualities point of view, the problem of a Bo105 helicopter rotor crossing, in low-speed level flight, the wake of an NREL 5MW wind turbine (WT), in the presence of atmospheric boundary layer (ABL). A crossing flight path orthogonal to the WT axis, and located two WT rotor diameters downstream to the WT disk, has been selected. Three different flight altitudes, with respect to the WT hub, and two flight directions, L2R and R2L, have been investigated. The aerodynamic simulations have been carried out by using a BEM methodology and by applying a decoupled interactional procedure specifically conceived for the purpose. The rotor blades have been assumed fully rigid. The simulations have shown that the encounter of a uniform side wind or a WT wake with a helicopter rotor, locally alters the velocities acting on the helicopter rotor blades, in magnitude and/or direction, because of the WT axial and radial changes in velocity deficit; the presence of the WT blade tip vortices; the presence of the ABL; the WT wake swirl. These velocities modify the helicopter rotor blade sectional effective angles of attack, which, in turn, change the blade loads, generate flapping angles and alter the rotor forces and moments. Compared to the flight inside a uniform side wind, the crossing of a WT wake produces important rotor rolling and pitching moments, the thrust increases while the torque decreases. The flight altitude has only moderate effects. Regarding the handling qualities, the paper has considered the ADS-33 pitch and roll attitude quickness parameters and has shown that when the WT wake approaches the helicopter from left to right (L2R) this results in an increase in the quickness that pilot needs to command. The analysis of the results has concluded that, for a WT rotor and helicopter rotor both counter-clockwise rotating, a pilot experiences a greater workload during the L2R crossing of the WT wake, but also that this situation is transient in nature and the pilot needs to command it only momentarily.

1 NOMENCLATURE

Symbol	Description	Units
c	Chord length	m
$CM_{x,y,z}$	Helicopter rolling, pitching, yawing moment coeffs. in the Air Frame of Reference (AFR)	
CQ	Helicopter rotor torque coeff.	
CT	Helicopter rotor thrust coeff.	
D_{WT}	Wind turbine rotor diameter	m
q_{pk}	Maximum pitch rate	deg/s
Q_{θ}	Attitude quickness parameter	1/s
R	Helicopter rotor radius	m
R_{WT}	Wind turbine rotor radius	m
u, v, w	Velocity components	m/s
V_H	Helicopter flight speed	m/s
WT	Wind Turbine	
X, Y, Z	Geometrical coordinates in AFR	m
α_{eff}	Effective angle of attack	deg
α_{sh}	Rotor shaft angle in AFR	deg
$\beta_0, \beta_{1c}, \beta_{1s}$	Conicity, longitudinal, lateral, flapping angles	deg
$\Delta\theta_{pk}$	Attitude angle change	deg
θ	Geometrical angle of attack	deg
$\theta_0, \theta_{1c}, \theta_{1s}$	Collective, lateral, longitudinal pitching angles	deg
μ	Helicopter advance ratio	

σ	Helicopter rotor solidity	
ψ	Blade azimuth position	deg
Ω_H, Ω_{WT}	Helicopter & WT rotor speeds	RPM

2 INTRODUCTION

The recent outlooks of the Global Wind Energy Council (GWEC)^[1] confirm the ever-increasing penetration levels of the wind power all over the world. In particular, the dramatic price reductions for off-shore wind is attracting the worldwide attention toward this technology, which is seen continuing to improve and spread beyond its home base in Europe in the next 5-10 years.

Performing maintenance operations at off-shore wind farms requires that all maintenance personnel and spare parts need to be transported from an on-shore port or station to the individual wind turbines (WT). These operations can be efficiently carried out by helicopters, thanks to their capability to hover and manoeuvre in confined areas. Furthermore, the rapid expansion of wind farms is also increasing the likelihood that helicopters, operating in both civil and military missions, can encounter the wake systems generated by WTs, often having large rotor diameters.

Literature describing fixed-wing aircraft or helicopters encounters with WT wakes is very limited. A study was carried out in 2014 at University of Liverpool^[2] in collaboration with the Civil Aviation Authority, UK, by using a modified Kocurek WT wake model, CFD, LIDAR field measurements and piloted flight simulations. The wake vortex model was applied to a WTN250 WT installed near the East Midlands Airport, UK and the velocities generated by the Kocurek wake vortex model were integrated into an aircraft flight dynamic model to simulate a WT wake

encounter with a light aircraft approaching an airport, where a WT was installed. The severity of the WT wake encounter was investigated using piloted flight simulations. The results suggested that the wake generated minor upsets on the aircraft and resulted in a severity rating of B if only the disturbances caused by wake velocity deficits were taken into account. The study also anticipated that if a helicopter encounter with the WT wake took place in the same fashion, the responses of the helicopter and pilots would be different due to different flight dynamics.

More recently, the specific problem of a WT tip vortex interacting with aircraft, gliders and helicopters has been systematically investigated, from the theoretical point of view, by van der Wall et alii in a set of publications where the wake of WT rotors was modelled as a tip vortex helix with a vortex strength estimated from its rotor thrust.

In van der Wall^[3,], a fixed-wing sail plane and a helicopter with a rotor represented as a fixed-wing circular disk were subjected to the wake. In both cases, the roll moment induced by the wake was compared to the maximum roll control moment of the aircraft. For comparison with rotating blades, the blade element momentum theory was applied to the isolated rotor and a simulation of an entire helicopter was used as well.

In van der Wall^[4,], helicopter rotors of different size and hub layout were subjected to the wake and the collective and cyclic control inputs required to keep the trim were compared to the maximum available control range of the rotorcraft. In addition, the blade flapping response, due to the vortex influence without pilot action, was computed and compared to the maximum allowed flapping angles.

The results of these two publications highlighted that typical on-shore power plants could be hazardous for sailplanes and ultra-light helicopters but not for larger ones. Large off-shore WTs were seen as a potential danger for small helicopters that may be used for maintenance.

In van der Wall^[5,] the aerodynamic impact of a straight-line vortex lying in the plane of a rotor disk was analytically solved by using the blade element/momentum theory and a realistic swirl velocity profile to evaluate the consequences on rotor thrust, blade aerodynamic hub moment, and collective and cyclic controls needed for disturbance rejection. Results were given for a rotor subjected to a wake vortex of a large aircraft and for that of a large WT.

With the aim to contribute to a more in-depth investigation of the interactional problem of "Wind Turbine Wake and Helicopter Operations", a GARTEUR action group – HC/AG-23^[6,] – was set up in 2014 by European researchers, from universities and research centres. The team performed computations and piloted simulator experiments, and analysed the effects of WT wake on the stability, handling qualities and safety aspects of a helicopter.

The present paper illustrates the numerical investigations carried out by CIRA and the Delft University of Technology in the framework of HC/AG-23, regarding the aerodynamic performance and handling qualities of a Bo105 helicopter rotor when immersed in the wake of the NREL 5MW WT.

3 SIMULATION TOOLS

3.1 BEM methodology

The aerodynamic computations have been carried out by using the code RAMSYS^[7,], which is an unsteady, inviscid and incompressible free-wake vortex lattice BEM solver for multi-body configurations developed at CIRA. It is based on Morino's boundary integral formulation for the solution of Laplace's equation for the velocity potential ϕ . The surface pressure distributions are evaluated by applying the unsteady version of Bernoulli equation, which is then integrated to provide the forces and moments on the helicopter configuration and the surrounding obstacles.

In order to account for the atmospheric boundary layer (ABL), a simple logarithmic law has been used in the computations, according to which the free stream velocity V_∞ at a height h is expressed as:

$$(1) \quad V_\infty(h) = V_\infty(h_{ref}) \left[\frac{\ln(h/z_0)}{\ln(h_{ref}/z_0)} \right]$$

where h_{ref} is a reference height, usually taken to be 10m above the ground, and z_0 is a roughness length depending on the type of terrain. In the present simulations an open country has been considered for which $z_0 = 0.02$ m.

The blade flapping induced by the interaction of the helicopter rotor with the WT wake has been referred to the rotor shaft plane, and has been evaluated by solving the ODE equation:

$$(2) \quad \ddot{\beta} + \Omega^2 v_\beta^2 \beta = \frac{M_\beta}{I_b}$$

where the nondimensional flapping frequency v_β is given in terms of the nondimensional flapping hinge offset e :

$$(3) \quad v_\beta = \sqrt{1 + \frac{3e}{2(1-e)}}$$

The flapping moment M_β has been obtained by integrating the equation:

$$(4) \quad M_\beta = \int_{eR}^R L(y - eR) dy$$

with L representing the blade lift, while the blade moment of inertia has been calculated by integration of equation:

$$(5) \quad I_b = \int_{eR}^R m(y - eR)^2 dy$$

3.2 Flight mechanics modelling

A flight mechanic model of the impact of the WT streamwise vortex on the rotor inflow has been built up and implemented. The helicopter flight path has been considered parallel to the WT rotor disk, and crossing the WT wake two WT rotor diameters downstream of the disk. Both the approaches of the helicopter to the WT wake on the main rotor (MR) port side (R2L - red colour) and on the MR starboard side (L2R - green colour), Figure 1, have been studied.

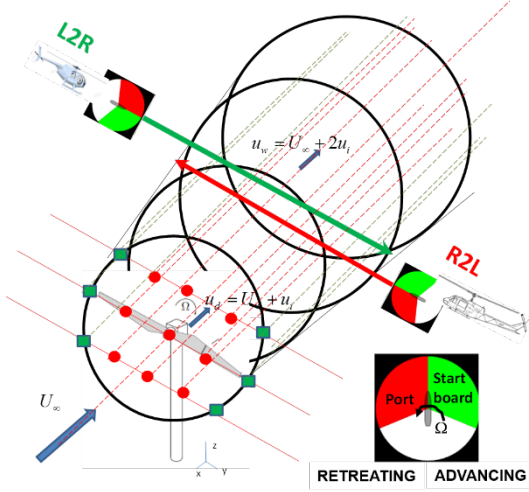


Figure 1: Description of the helicopter approaching the WT wake

On the helicopter rotor disk plane the representation of the incoming vortex and the rotor would be as shown in Figure 2, where the red dashed circle represents the vortex and the blue circle is the rotor, respectively. It is assumed that the helicopter is flying forward at a velocity V and α_d is the angle of attack with respect to the disk plane. The impinging position of the vortex is located at point C , at a radial distance r_c from the rotor centre; the tangential velocity of the vortex is $U_{t,C}$ and the circulation is Γ_∞ . The rotor centre is located at O ; the rotor speed is Ω and counter-clockwise; a point P on the blade is situated at a distance r . The induced velocities of the vortex can be projected in the tangential and radial directions of the rotor blade and are represented by $U_{t,i}$ and $U_{r,i}$, respectively. The rotation direction of the vortex is the same as that of the rotor speed, so the vortex is denoted as a co-rotating vortex as indicated in Figure 2.

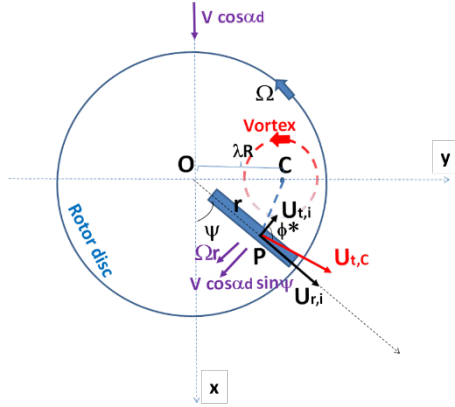


Figure 2: Induced velocities on the rotor due to a vortex. Rotor up view

Referring to Figure 2 the figure, the induced tangential velocity on the blade element due to the vortex is formulated as:

$$(6) \quad U_{t,i} = U_{t,C} \cos \varphi^*$$

where φ^* has the same value as \widehat{CPD} , i.e.:

$$(7) \quad \cos \varphi^* = \frac{PC^2 + PO^2 - CO^2}{2PC \cdot PO}$$

The distances are defined as:

$$(8) \quad PC = \sqrt{(r \cos \psi)^2 + (r_c - r \sin \psi)^2}$$

$$(9) \quad PO = r = \sqrt{(r \cos \psi)^2 + (r \sin \psi)^2}$$

$$(10) \quad CO = r_c$$

It follows that the total tangential and perpendicular components of the velocities on the blade element are:

$$(11) \quad U_p = V \sin \alpha_d + v_i + \dot{\beta} r + \beta V \cos \alpha_d \cos \psi - qr \cos \psi - pr \sin \psi$$

$$(12) \quad U_T = \Omega r + V \cos \alpha_d \sin \psi m U_{t,i}$$

where v_i represents the rotor inflow which will be assumed constant in a flight condition. These equations assume that the blade is flapping with an angle β , the helicopter is having a pitch rate q and a roll rate p . The sign m in $mU_{t,i}$ was introduced to represent the multitude of situations where the vortex can impinge on the rotor disk and corresponds to a minus when the helicopter comes from left to right (L2R) towards the wake (the vortex attacks the blade advancing side) and to a plus when the helicopter comes from right to left (R2L) on the wind turbine wake (the vortex attacks the blade retreating side). For the case of Figure 2 the sign is minus. The vortex creates an extra angle of attack, Figure 3, which can be expressed as:

$$(13) \quad \begin{aligned} \Delta \alpha &= \alpha^* - \alpha = (\theta - \varphi^*) - (\theta - \varphi) \\ &= -\frac{U_p}{U_T m U_{t,i}} + \frac{U_p}{U_T} \\ &= m \frac{U_p}{U_T} \frac{U_{t,i}}{U_T m U_{t,i}} \\ &= m \varphi \frac{U_{t,i}}{U_T m U_{t,i}} \end{aligned}$$

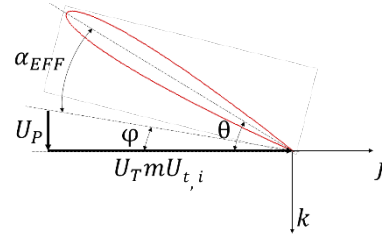


Figure 3: Angle of attack of blade element

This results in a change of lift as:

$$(14) \quad \Delta L = \frac{1}{2} \rho (U_T^*)^2 Cl_\alpha \Delta \alpha c dr = \frac{1}{2} \rho m Cl_\alpha U_p U_{t,i} c dr$$

and a change in the pitch moment:

$$(15) \quad \begin{aligned} \Delta M &= \int_0^R \Delta L r = \int_0^R \frac{1}{2} \rho (U_T^*)^2 Cl_\alpha \Delta \alpha c r dr \\ &= m \int_0^R \frac{1}{2} \rho Cl_\alpha U_p U_{t,i} c r dr \end{aligned}$$

Integrating and using non-dimensional notations, the change in blade pitch moment due to WT vortex can be expressed as:

$$(16) \quad \Delta M = \frac{1}{2} \gamma I_b \Omega^2 (m \bar{U}_{t,i}) \left[\frac{1}{2} (\lambda_c + \lambda_i) + \frac{1}{3} \dot{\beta}' - \frac{1}{3} (\bar{q} \cos \psi - \bar{p} \cos \psi) + \frac{1}{2} \beta \mu \cos \psi \right]$$

where the non-dimensional notations are: Lock number $\gamma = \frac{\rho C l \alpha_c R^4}{I_b}$; advance ratio $\mu = \frac{v \cos \alpha_c}{\Omega R}$ when expressed with respect to the control plane; $\lambda_c = \frac{v \sin \alpha_c}{\Omega R}$; non-dimensional inflow $\lambda_i = \frac{v_i}{\Omega R}$; $\bar{U}_{T,i} = \frac{U_{T,i}}{\Omega R}$; $\bar{q} = \frac{q}{R}$; $\bar{p} = \frac{p}{R}$.

The change in blade flapping for the helicopter flying forward flight can be written as:

$$(17) \quad \Delta \ddot{\beta} + \frac{\gamma}{8} \Omega \Delta \dot{\beta} \left[1 + \frac{4}{3} \mu \sin \psi \right] + \Omega^2 \Delta \beta \left[v_\beta^2 + \frac{\gamma}{6} \mu \cos \psi + \frac{\gamma}{8} \mu^2 \sin 2\psi \right] = \frac{\Delta M}{I_b}$$

In the non-rotating frame, assuming a Fourier expression for the flapping angle and considering no flapping dynamics, it follows that:

$$(18) \quad \begin{aligned} \Delta \beta &= \Delta \beta_0 + \Delta \beta_{1c} \cos \psi + \Delta \beta_{1s} \sin \psi \\ \Delta \dot{\beta} &= -\Omega \Delta \beta_{1c} \sin \psi + \Omega \Delta \beta_{1s} \cos \psi \\ \Delta \ddot{\beta} &= -\Omega^2 \Delta \beta_{1c} \cos \psi + \Omega^2 \Delta \beta_{1s} \sin \psi \end{aligned}$$

Substituting Eq.(18) into Eq.(17) and expressing $\bar{U}_{T,i}$ as a function of the tangential velocity of the vortex $\bar{U}_{T,c}$, see Eq.(6), the change in flapping angles as a result of the helicopter encountering the WT wake are given as:

$$(19) \quad \Delta \beta_{1c} = 4 \left(\frac{N_1 + N_2}{D_1 + D_2} \right)$$

$$(20) \quad \Delta \beta_0 = \frac{\gamma (\lambda_c + \lambda_i) \bar{U}_{1T}}{2v_\beta^2} - \frac{\gamma \mu \left(\frac{1}{3} + \bar{U}_{1T} \right)}{v_\beta^2} \cdot \left(\frac{N_1 + N_2}{D_1 + D_2} \right)$$

$$(21) \quad \Delta \beta_{1s} = \frac{\gamma \bar{U}_{2T} p}{2(v_\beta^2 - 1)} + \frac{\gamma \left(1 - \frac{\mu^2}{2} + 4\bar{U}_{2T} \right)}{2(v_\beta^2 - 1)} \cdot \left(\frac{N_1 + N_2}{D_1 + D_2} \right)$$

with the terms N_1, N_2, D_1, D_2 expressed as:

$$N_1 = -\gamma v_\beta^2 \left(1 + \frac{\mu^2}{2} + 4\bar{U}_{2T} \right) \bar{U}_{2T} p$$

$$N_2 = 8v_\beta^2 (v_\beta^2 - 1) \bar{U}_{2T} q + 4\gamma \mu (v_\beta^2 - 1) \left(\frac{1}{3} - \bar{U}_{1T} \right) \bar{U}_{1T} (\lambda_c + \lambda_i)$$

$$D_1 = 16\mu v_\beta^2 (v_\beta^2 - 1) \left(\frac{1}{3} + \bar{U}_{1T} \right) - \gamma v_\beta^2 \left[\left(1 - \frac{\mu^2}{2} \right)^2 + 8\bar{U}_{2T} + 16\bar{U}_{2T}^2 \right]$$

$$D_2 = 8\gamma \mu^2 (v_\beta^2 - 1) \left(\frac{1}{9} - \bar{U}_{1T}^2 \right)$$

where $\bar{r}_c = \frac{r_c}{R}$ and the following expressions are used for velocities $\bar{U}_{1T} = m \bar{U}_{1c} \left| \frac{1}{3} - \frac{1}{2} \bar{r}_c \right|$ and $\bar{U}_{2T} = m \bar{U}_{1c} \left| \frac{1}{4} - \frac{1}{3} \bar{r}_c \right|$.

4 WIND TURBINE AND HELICOPTER ROTOR MODELS

In accordance with the work programme of the HC/AG-23 project, the simulations have been made by considering the model NREL 5MW WT and the main rotor of the Bo105 helicopter. The main characteristics of these two configurations are summarized in the following:

4.1 NREL 5-MW baseline wind turbine

This model WT is heavily based on the REpower 5M machine, Figure 4, and makes also use of publicly available properties from the conceptual models in the WindPACT, RECOFF, and DOWEC projects. It is a conventional three-bladed upwind variable-speed variable blade-pitch-to-feather-controlled turbine. The main properties are summarized in Table 1, while the details can be found in NREL^[8].



Figure 4: REpower 5M WT

Description	Value
Rating	5 MW
Rotor Orientation, Configuration	Upwind, 3 Blades
Rotor; Hub Diameter	126 m; 3 m
Hub Height	90 m
Cut-In; Rated; Cut-Out Wind Speed	3 m/s, 11.4 m/s, 25 m/s
Cut-In; Rated Rotor Speed	6.9 RPM, 12.1 RPM
Overhang; Shaft Tilt; Pre-cone	5 m, 5°, 2.5°

Table 1: NREL 5-MW WT main characteristics

4.2 Bo105 helicopter

The Bo105 is a small multipurpose helicopter built by MBB (now Airbus Helicopters) and it is powered by two Allison 250 C20 engines. It is a relatively small helicopter with an empty weight of about 1200kg and a maximum gross

weight of 2300kg. Typical uses of the highly manoeuvrable Bo105 helicopter are transport, off-shore, police, and military missions. The Bo105 has a hingeless main rotor with four rectangular blades, constituted by a NACA23012 airfoil, and a two-bladed teetering tail rotor. The main properties are summarized in Table 2, while the details can be found in Lehmann^[9].



Figure 5: Bo105 helicopter

Description	Value
Radius, R	4.912 m
Rotor speed, Ω	424 RPM
Blade chord, c	0.27 m
Number of blades	4
Precone angle, β_0	2.5 deg
Main rotor shaft tilt, α_{sh}	-3.0 deg
Non dimensional flapping frequency, ν_β	1.117
Absolute flapping hinge offset, eR	0.746 m
First aerodynamic section (22%R)	1.1 m
Twist (linear), θ_{tw}	-6.2 deg
Effective blade mass, M	24.2 kg

Table 2: Main characteristics of the Bo105 main rotor

5 DECOUPLED INTERACTIONAL PROCEDURE

The interactional procedure implemented for the present investigations has been conceived by taking into account the considerably different characteristic times for the WT and helicopter rotor wake to develop. Indeed, because of the respective rotor speeds, the helicopter rotor is approximately 35 times faster than the WT rotor, when the rated condition for the latter one is considered. Since experience indicates that for a level forward flight a fairly time-accurate BEM simulation requires a blade azimuth step of 5° at least, this would imply a WT blade azimuth step not greater than about 0.14° , a resolution impractical also in consideration of the many WT rotor revolutions required to model a sufficiently developed wake length.

A decoupled interactional procedure has been therefore set up, consisting of the following three main steps:

1. evaluation of the WT wake development in absence of the helicopter rotor;
2. evaluation of a time-averaged WT wake flow field in a box located downstream of the WT disk, at the station where the interaction with the helicopter rotor takes place;
3. evaluation of the helicopter rotor flow field and loads, when immersed in the time-averaged WT wake flow field.

3. evaluation of the helicopter rotor flow field and loads, when immersed in the time-averaged WT wake flow field.

5.1 WT wake development evaluation

The WT rated condition has been selected for the numerical simulations. This corresponds to a rotor speed $\Omega_{WT} = 12.1$ RPM and to a wind speed $V_\infty = 11.4$ m/s. The rotor shaft α_{sh} is set at 5° and the blade pre-cone angle β_0 is -2.5° . The blades have no pitch angle. A counter-clockwise rotor speed (when observed from upstream) has been considered in the simulations.

The blades and pylon have been assumed to be fully rigid, whereas no nacelle has been modelled. Each blade has been discretised by 640×16 panels, and 1080 panels have been used to model the pylon. Twelve rotor revolutions have been considered for the generation of the wake. A time discretization corresponding to an azimuth step $\Delta\psi = 5^\circ$ has been used.

No turbulence has been taken into account.

Figure 6 illustrates the main characteristics of the wake development in the presence of ABL: Figure 6a shows the ABL logarithmic law; Figure 6b gives a perspective view of the wake, and a side view is shown in Figure 6c where only root and tip vortices have been represented.

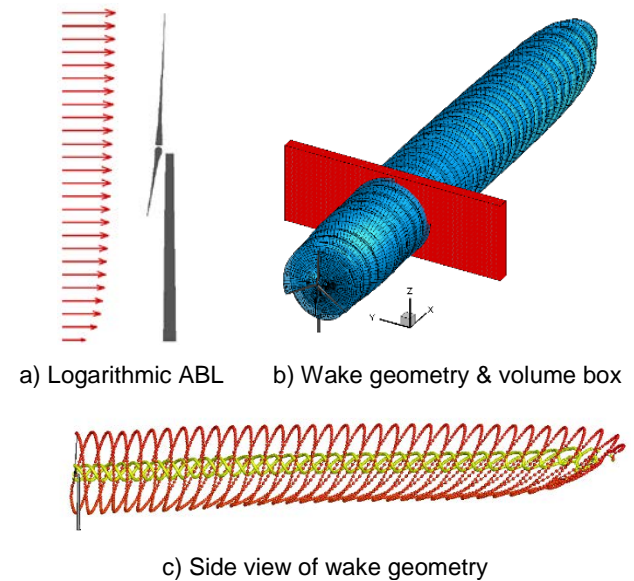


Figure 6: WT wake development in presence of ABL

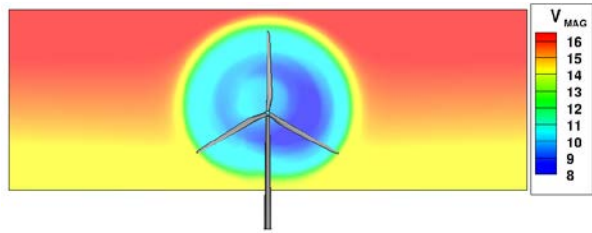
5.2 Computational volume box

During the evaluation of the WT wake development, the velocities induced in a region of space located two WT rotor diameters downstream of the WT rotor disk ($X = 252$ m), have been calculated at each time step during the last rotor revolution. This region has been bounded by a box having its centre in the WT rotor hub ($Y_{WT \text{ Hub}} = 0$; $Z_{WT \text{ Hub}} = 90$ m) and extending about 3 WT rotor diameters in the Y direction; 140 m in height Z, starting from 30 m above the ground; 20 m in the axial direction X, Figure 6b.

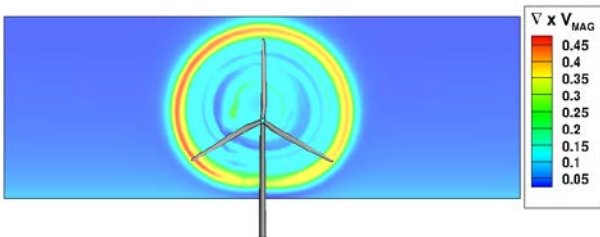
A space resolution of 1 m in all the three directions has been chosen to discretize the volume box.

This calculation has generated 72 volume boxes containing instantaneous velocity fields that have been time-averaged in order to create a single volume box that has been used for the decoupled interactional procedure with the helicopter flow field.

The time-averaged flow field is shown in Figure 7 in terms of velocity and vorticity magnitudes evaluated at $X = 2D_{WT}$. Figure 7a highlights the increasing velocity with height, due to the ABL, and the velocity deficit inside the WT wake, which is significantly lower than the free stream in the region corresponding to the mid-span advancing blade. The vorticity magnitude highlights the strong influence of the tip vortices, Figure 7b.



a) Velocity field



b) Vorticity field

Figure 7: Time-averaged flow field at $X = 2D_{WT}$

Figure 8 provides indications of the velocity deficit inside the WT wake. In particular, Figure 8a compares the logarithmic ABL velocity profile with the one evaluated in the wake at the hub radial station $Y_{WT} / R_{WT} = 0$. Figure 8b shows the Y distribution of velocity deficit in the wake at three different heights with respect to the rotor hub: $Z = Z_{Hub} - R_{WT}/2 = 60$ m; $Z = Z_{Hub} = 90$ m; $Z = Z_{Hub} + R_{WT}/2 = 120$ m.

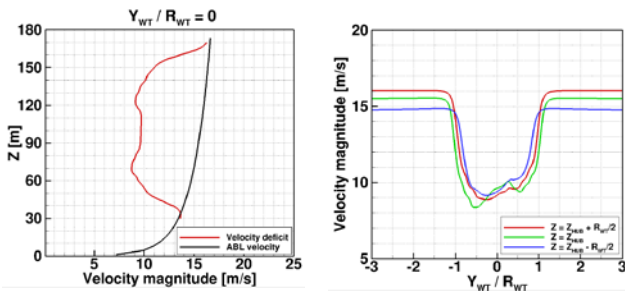


Figure 8: Velocity deficit in the WT wake

5.3 Helicopter rotor and flight condition

The low-speed level flight, DPt. 344, has been selected from the experimental database of the HELINOISE project^[10,1] as reference flight condition for the helicopter rotor. Despite it refers to a wind tunnel test, wind tunnel corrections had been introduced to correspond to a real full-scale flight condition. The advance ratio is $\mu = 0.15$ and the flight speed is $V_H = 32.75$ m/s. The rotor has been trimmed in order to have zero flapping with only a pre-cone angle β_0 set at 2.5° . The pitch angles are $\theta_0 = 5.35^\circ$, $\theta_{1c} = -1.58^\circ$, $\theta_{1s} = 1.48^\circ$. The shaft angle α_{sh} includes the wind tunnel correction angle and is equal to -2.46° . These values provide a thrust coefficient CT equal to 0.00446.

The four rotor blades have been considered fully rigid and have been discretized by 60×16 panels per blade. Four spirals have been used to model the wake, and four rotor revolutions have been necessary to obtain a converged thrust coefficient, Figure 9. The experimental pitch angles have been used for the numerical simulations, with the exception of the collective pitch θ_0 that has been adjusted to 5.14° in order to obtain, on average, the same experimental thrust coefficient, Figure 10.

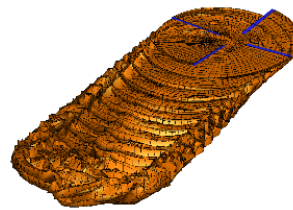


Figure 9: Wake development

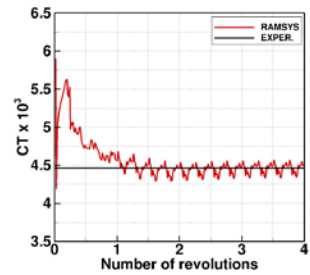


Figure 10: Thrust coefficient time history

6 WIND TURBINE/HELICOPTER INTERACTION

The simulations of interactional aerodynamics have been performed on four different flight conditions:

1. Nominal condition: flight in undisturbed atmosphere;
2. Hover condition;
3. Uniform side wind condition;
4. WT wake crossing.

For all computations, the experimental trim values of the nominal flight condition have been used (with the only correction applied to the collective pitch in order to obtain the experimental thrust coefficient) and no re-trim has been performed. The only induced components of the forces and moments have been calculated at the rotor hub and on each blade. The latter calculations have been used in order to evaluate, as a post-process, the dynamics of blade flapping by solving Eq.(2). Despite higher harmonics have arisen from the solution, only the conicity and the first harmonics terms have been considered.

The map of the simulated test conditions is shown in Figure 11.

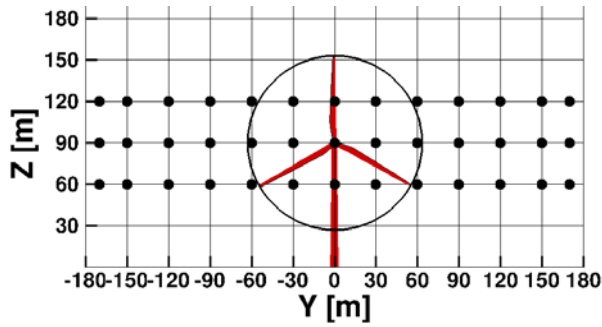


Figure 11: Map of the selected test conditions

They have been selected with the aim to investigate the effect on the helicopter rotor performance of the:

- height Z from the ground surface. Three altitudes have been considered: $Z = Z_{Hub} - R_{WT}/2 = 60$ m; $Z = Z_{Hub} = 90$ m; $Z = Z_{Hub} + R_{WT}/2 = 120$ m, in order to measure the changes in performance produced by the combined effect of the WT wake swirl and the different wind speed inside the ABL;
- Y station while crossing the WT wake. The helicopter radial positions have been varied, in static conditions (no flight dynamics involved), from $R = -170$ m (circa $-2.70 R_{WT}$) to $R = 170$ m (circa $2.70 R_{WT}$), with the aim to investigate the effect of the WT wake swirl on the helicopter performance;
- flight path direction. As indicated in Figure 1, the helicopter has been flown both in the direction leaving the WT rotor disk on its port side (R2L), and in the one leaving the WT rotor disk on its starboard side (L2R). The aim was to investigate the effect of the WT wake encounter when coming from both the helicopter rotor retreating and advancing blade sides, respectively.

6.1 Nominal condition

The calculations for the nominal flight condition have been carried out by using the parameters specified in section 5.3, which have produced the flapping angles, forces and moments shown in Table 3. These values have been then used as reference data for the calculation in uniform side wind speed.

Nominal			
β_0 [deg]	3.30	$CQ \times 10^4$	1.14
β_{1c} [deg]	-0.71	$CM_{Roll} \times 10^2$	1.38
β_{1s} [deg]	1.45	$CM_{Pitch} \times 10^2$	0.62
$CT \times 10^3$	4.46	$CM_{Yaw} \times 10^2$	-0.96

Table 3: Flapping angles, thrust and moment coefficients of a rotor in level flight in nominal conditions

6.2 Hover condition

Before the simulation of the level flight condition, preliminary computations have been performed in hover, in order to provide an easier explanation of the fundamental aspects of the interactional phenomenology when crossing a WT wake. These computations have dealt with the rotor flying both in undisturbed atmosphere and when subjected to a side wind of uniform speed.

When a wind comes from the port side of the rotor R2L, the presence of a conicity angle generates an upwash on the retreating blade, which increases the effective angle of attack, and a downwash on the advancing blade, which reduces the effective angle of attack. The net result is a negative rolling moment. The converse happens when the wind comes from the starboard side L2R of the rotor and the net result is a positive rolling moment, Figure 12.

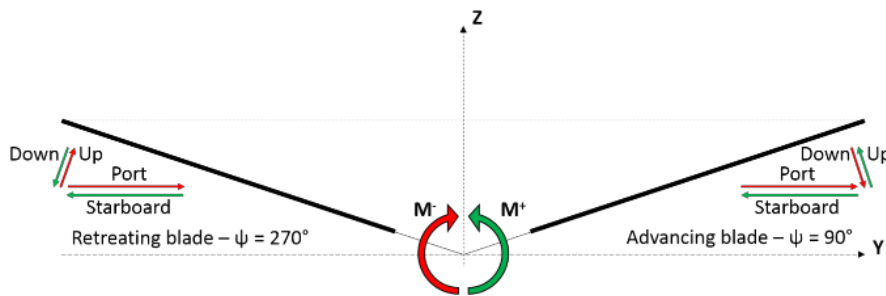


Figure 12: Effect of a uniform side wind on the rotor rolling moment

At the same time, when a uniform wind impinges the rotor from R2L, the tangential velocity V_T , compared to the nominal condition of hover in undisturbed atmosphere, Figure 13a, increases on the forward part of the disk, causing an increase in the effective angle of attack, and

decreases on the backward part, causing a reduction of the effective angle of attack, Figure 13b, thus producing a positive pitching moment. The converse happens when the side wind comes from L2R, and a negative pitching moment is generated, Figure 13c.

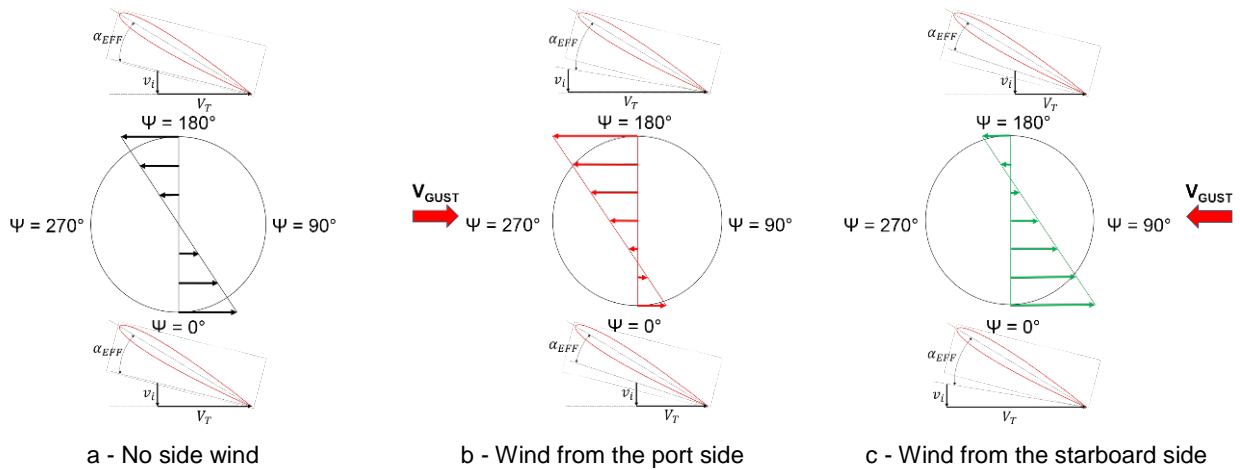


Figure 13: Changes in the blade effective angle of attack induced by a uniform side wind in hover

These results are confirmed by the changes in the flapping angles, thrust and moments coefficients, as summarized in Table 4, and by the changes occurring, at a given blade section, in the effective angle of attack during a rotor revolution, Figure 14.

	Nominal	Uniform side wind	
		Port side	Starboard
β_0 [deg]	3.78	4.53	4.53
β_{1c} [deg]	0.00	-3.44	3.44
β_{1s} [deg]	0.00	-6.76	6.76
CT x 10 ³	4.86	5.84	5.84
CQ x 10 ⁴	4.07	4.03	4.03
CM _{Roll} x 10 ⁴	0.00	-6.79	6.79
CM _{Pitch} x 10 ⁴	0.00	5.61	-5.61
CM _{Yaw} x 10 ⁴	-4.07	-4.03	-4.03

Table 4: Changes in the flapping angles, thrust and moment coefficients of a rotor in hover, induced by a uniform side wind

In particular, the effect of a side wind, compared to the nominal condition, is to increase the conicity β_0 and to generate longitudinal, β_{1c} , and lateral, β_{1s} , flapping angles, which are equal in module but opposite in sign, depending on the direction of the side wind. The thrust is increased, whereas the torque is almost unchanged. Both roll and pitching moments are generated by the side wind, and both are equal in module but opposite in sign, depending on the direction of the wind. Finally, since an isolated rotor is considered and the pole coincides with the rotor hub, the yawing moment is equal to the torque in module, but opposite in sign because of the opposite notation used for the moment about the z-axis of the rotor and of the aircraft, respectively.

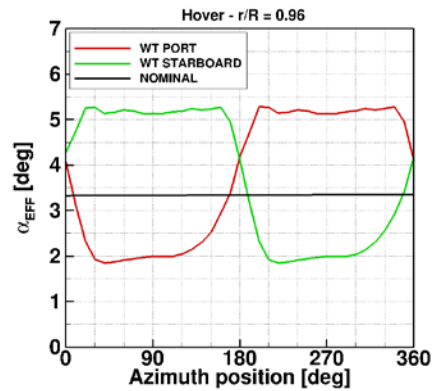


Figure 14: Time history of the blade effective angle of attack at $r/R = 0.97$ in hover with and without uniform side wind

6.3 Uniform side wind condition

This condition has been investigated with the aim to highlight the effect of the ABL, without considering any contribution induced by the WT wake. The results have been represented in terms of differences with respect to those of the nominal condition. In general, the different heights have produced almost negligible effects.

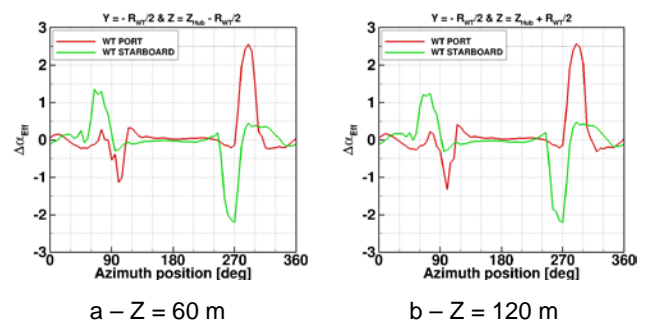


Figure 15: Time history of the blade effective angle of attack variation at $r/R = 0.97$ referred to the nominal condition.

Figure 15 shows the variation of the effective angle of attack in the radial station $r/R = 0.97$, at two heights, $Z = 60$ m and 120 m, in both the flight directions RL2 and L2R. The side wind impingement produces its greatest effect around $\psi = 90^\circ$ and $\psi = 270^\circ$, where the helicopter rotor blades are aligned with the side wind velocity. The direction of flight provides opposite results in terms of both peak magnitude, and peak location with respect to the azimuth positions $\psi = 90^\circ$ and $\psi = 270^\circ$.

The variation of the blade flapping angles with respect to the nominal conditions are illustrated in Figure 16. The direction of flight determines clear differences on the cyclic flapping angles, which are both reduced when the side wind impinges the helicopter from R2L, and increased, almost of the same quantity, when the side wind impinges the helicopter from L2R. The differences in conicity follow the same behaviour as the cyclic angles but the changes in absolute values are one order of magnitude lower

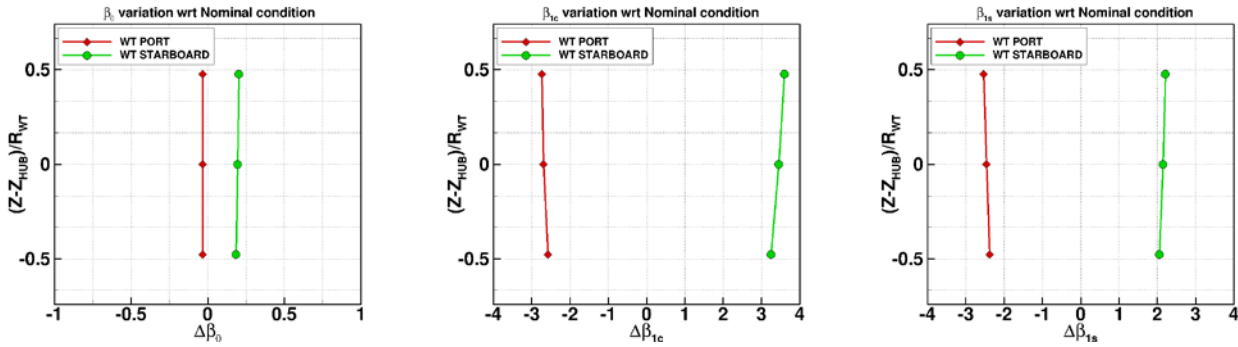


Figure 16: Variation of the blade flapping angles with respect to the nominal conditions at the heights 60 m, 90 m, 120 m, respectively. Uniform side wind coming from R2L (red) or L2R (green).

The variation with respect to the nominal conditions of the hub moments are shown in Figure 17. They are the direct consequence of the flapping angles variations. More specifically, the variations of the longitudinal cyclic flapping angle $\Delta\beta_{1c}$ produce a variation of the pitching moment ΔCM_y , which reduces when the side wind impinges the

helicopter from L2R, and increases, of almost the same quantity, when the side wind impinges the helicopter from R2L. The opposite behaviour can be observed for the variation of the rolling moment ΔCM_x , which is produced by the variation of the lateral cyclic flapping angle $\Delta\beta_{1s}$. The yawing moment remains almost unvaried.

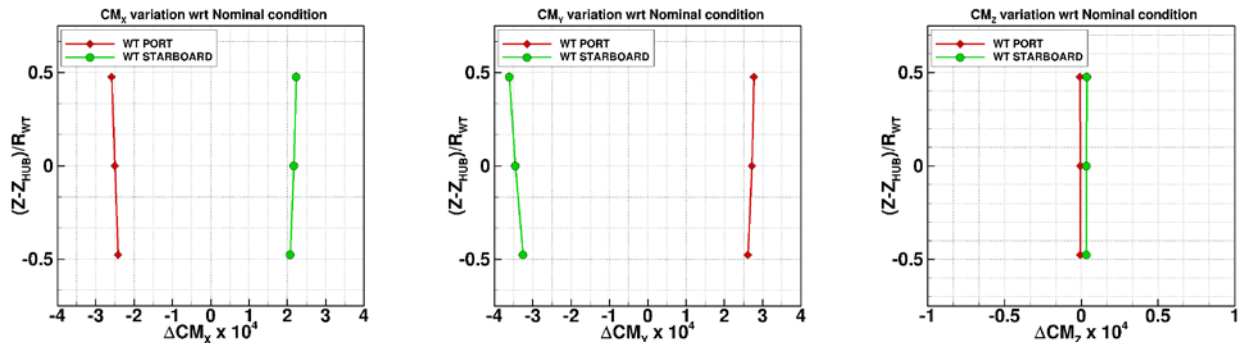


Figure 17: Variation of the helicopter moment coefficients with respect to the nominal conditions at the heights 60 m, 90 m, 120 m, respectively. Uniform side wind coming from R2L (red) or L2R (green).

The variation with respect to the nominal conditions of the thrust and torque are shown in Figure 18. Both quantities slightly reduce when the side wind impinges the helicopter

from R2L, and increase, of a slight higher value, when the side wind impinges the helicopter from L2R.

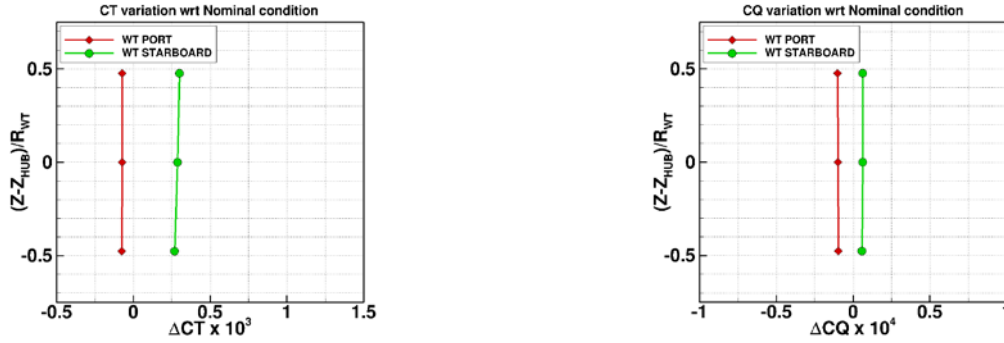


Figure 18: Variation of the rotor thrust (left) and torque (right) coefficients with respect to the nominal conditions at the heights 60 m, 90 m, 120 m, respectively. Uniform side wind coming from R2L (red) or L2R (green).

6.4 WT wake crossing

When a helicopter crosses a WT wake, the interactional phenomenology is more complex. The helicopter rotor is subjected to locally variable velocities, in magnitude and/or direction, because of the axial and radial changes in velocity deficit; the presence of the WT blade tip vortices; the presence of the ABL; the wake swirl. These variable velocities induce on the helicopter variable loads that are determined by the changes in the effective angle of attack that occur along the blade span of the helicopter rotor. Figure 19 shows the details of the effective angle of attack variations, at the radial station $r = 0.97R$, during one revolution of the rotor flying below the WT hub, at a height from the ground of 60 m.

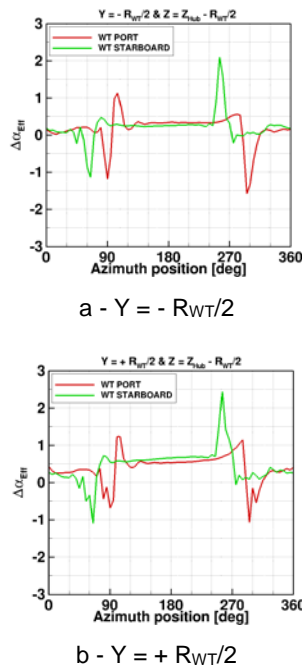


Figure 19: Time history of the blade effective angle of attack variation at $r/R = 0.97$ compared to the uniform side wind condition at height 60 m.

The changes in the effective angles of attack have produced variations of the flapping angles and, in turn, of the loads and moments acting on the rotor.

The general trends observed during the interaction with the uniform side wind, Figure 15, also hold during the interaction with the WT wake. However, some remarkable differences have been observed: compared with the flight in uniform side wind, the interaction with the WT wake produces a general increases in the effective angle of attack, particularly in the forward part of the helicopter rotor disk, and particularly in the region of the WT blade retreating side, $Y = +R_{WT}/2$. In addition, during the flight from R2L, the effective angle of attack shows significant fluctuations around the azimuth position $\psi = 90^\circ$ of the helicopter rotor blade.

The global characteristics shown for the flight at 60 m are also kept during the flight at 120 m, Figure 20.

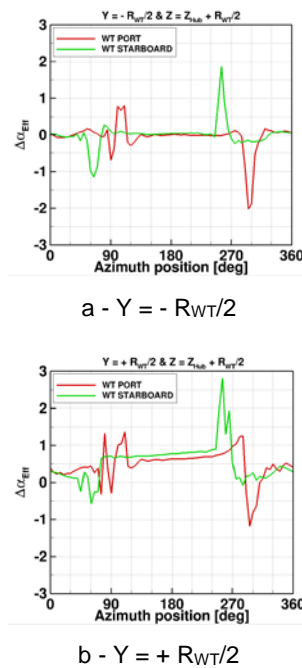


Figure 20: Time history of the blade effective angle of attack variation at $r/R = 0.97$ compared to the uniform side wind conditions at height 120 m.

Figure 21 describes the flapping angle variations, at the three selected flight heights, for the helicopter flying in both directions with respect to the WT rotor disk. They are referred to the uniform side wind condition.

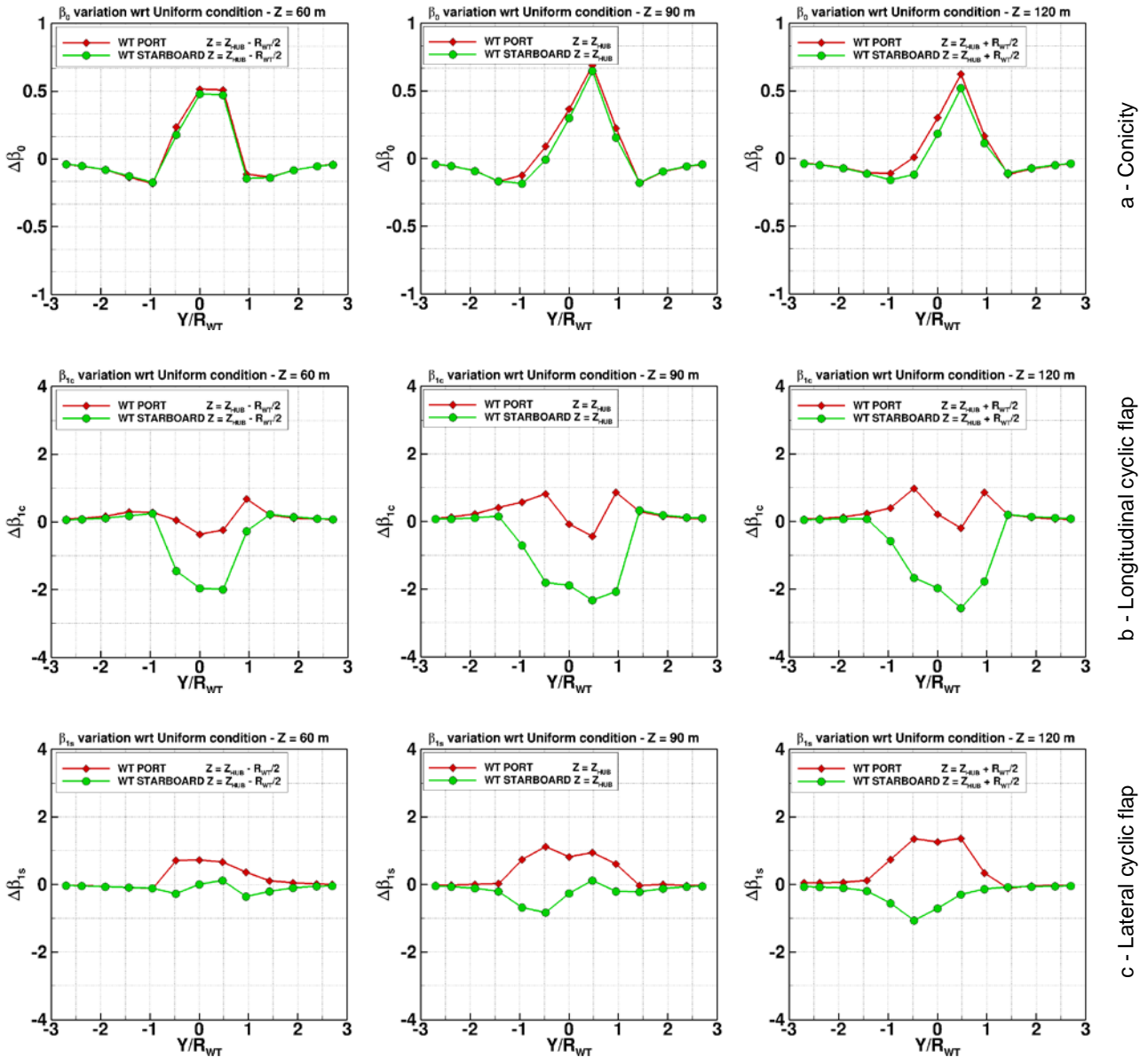


Figure 21: Variation of the flapping angles with respect to the uniform conditions at the heights 60 m, 90 m, 120 m, respectively. Helicopter leaving the WT disk on its port side R2L (red) or starboard side L2R (green) while crossing the WT wake

Since the WT wake enlarges downstream of the WT rotor disk, a general characteristic is that the helicopter rotor feels the influence of the WT wake in a region that radially extends for more than the WT rotor radius, about $1.5R_{WT}$.

Figure 21a illustrates the changes in conicity, $\Delta\beta_0$. This increases of less than 1° inside the WT wake, regardless of the direction of flight. Figure 21b shows the changes in longitudinal cyclic flap, $\Delta\beta_{1c}$. Following the phenomenological explanation described in section 6.2, the WT wake produces a considerable reduction (about 2°) of this flap angle during the flight in the direction L2R, which increases with height and is generally located in a region around the WT rotor hub. Conversely, during the

flight in the direction R2L, the WT wake produces an oscillating behaviour of this flapping angle with an average increase of about 0.5° but with a negative peak between $Y/R_{WT} = 0.0$ and 0.5 . Finally, Figure 21c shows the changes in lateral cyclic flap, $\Delta\beta_{1s}$. In this case, the variations are lower than the longitudinal cyclic flap (in a range between -1° and 1.5°), increasing with the height, and mostly inverted, with respect to longitudinal cyclic flap, as far as the direction of flight is concerned.

These variations in the flap angles have produced variations in the hub moments that are illustrated in Figure 22.

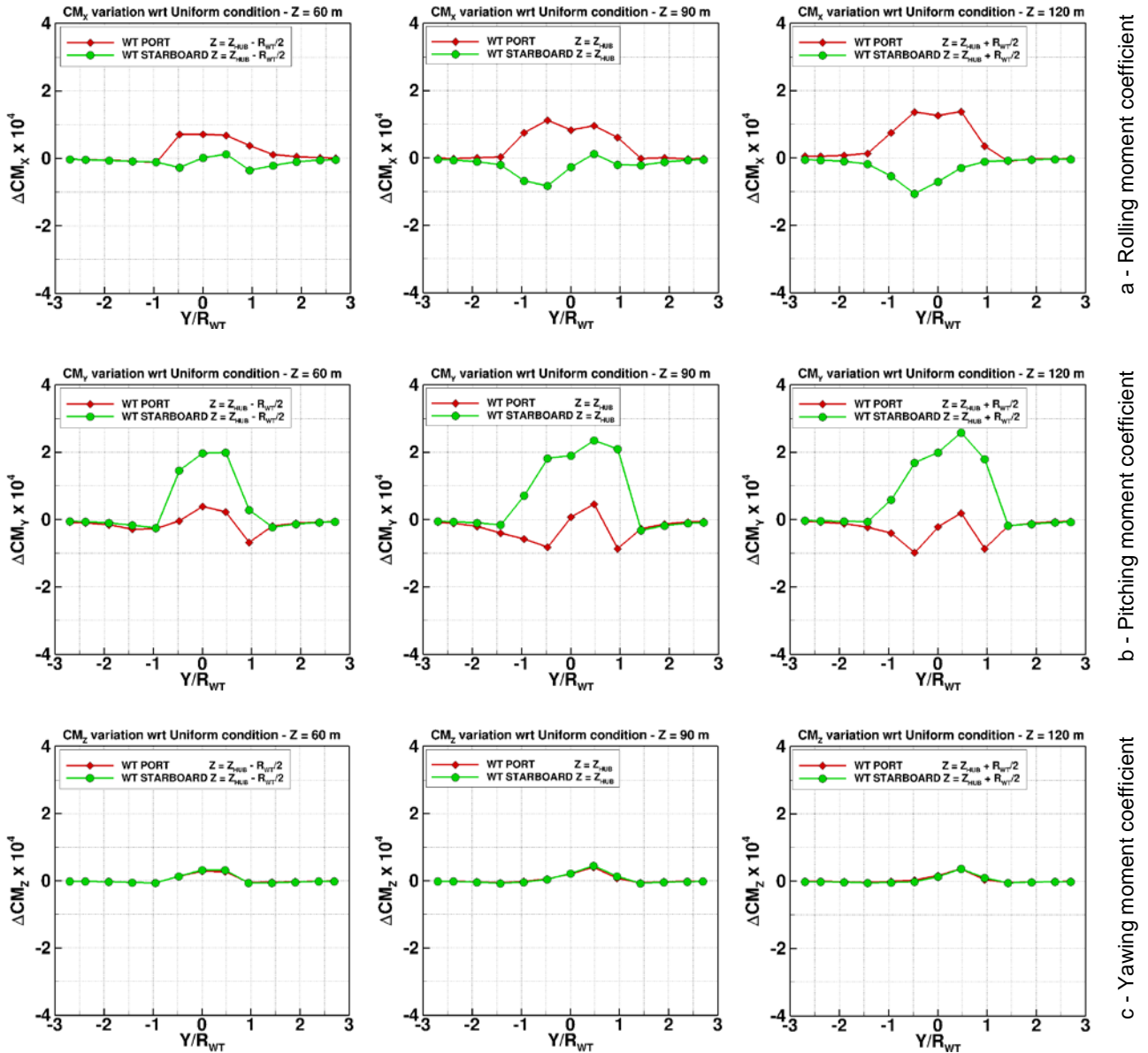


Figure 22: Variation of the helicopter moment coefficients with respect to the uniform conditions at the heights 60 m, 90 m, 120 m, respectively. Helicopter leaving the WT disk on its port side R2L (red) or starboard side L2R (green) while crossing the WT wake

In particular, despite inverted if referred to the flight path directions, the changes in the longitudinal cyclic flap $\Delta\beta_{1c}$ have produced the same qualitative changes in the pitching moments ΔCM_y , Figure 22b, whereas the changes in the lateral cyclic flap $\Delta\beta_{1s}$ have produced the same qualitative changes in the rolling moments ΔCM_x , Figure 22a. Similarly, the qualitative behaviour of the yawing moment variation ΔCM_z has reproduced the one of the concity variation $\Delta\beta_0$.

Figure 23 shows the changes in the helicopter rotor thrust and torque coefficients. The first increases during the WT

wake crossing, while the latter reduces. In both cases there is an inversion in the behaviour while crossing the WT wake: the thrust variations first reduce while approaching and leaving the WT wake, than increase inside the wake reaching a maximum at a distance from the WT rotor hub of $Y/R_{WT} = 0.5$; the opposite can be observed for the torque variation. The flight direction determines only minor differences in both coefficients, with slightly higher values in thrust and slightly lower ones in torque for the WT port side flight. The height produces small differences but the flight at 90 m generates higher thrust and more negative torque variations.

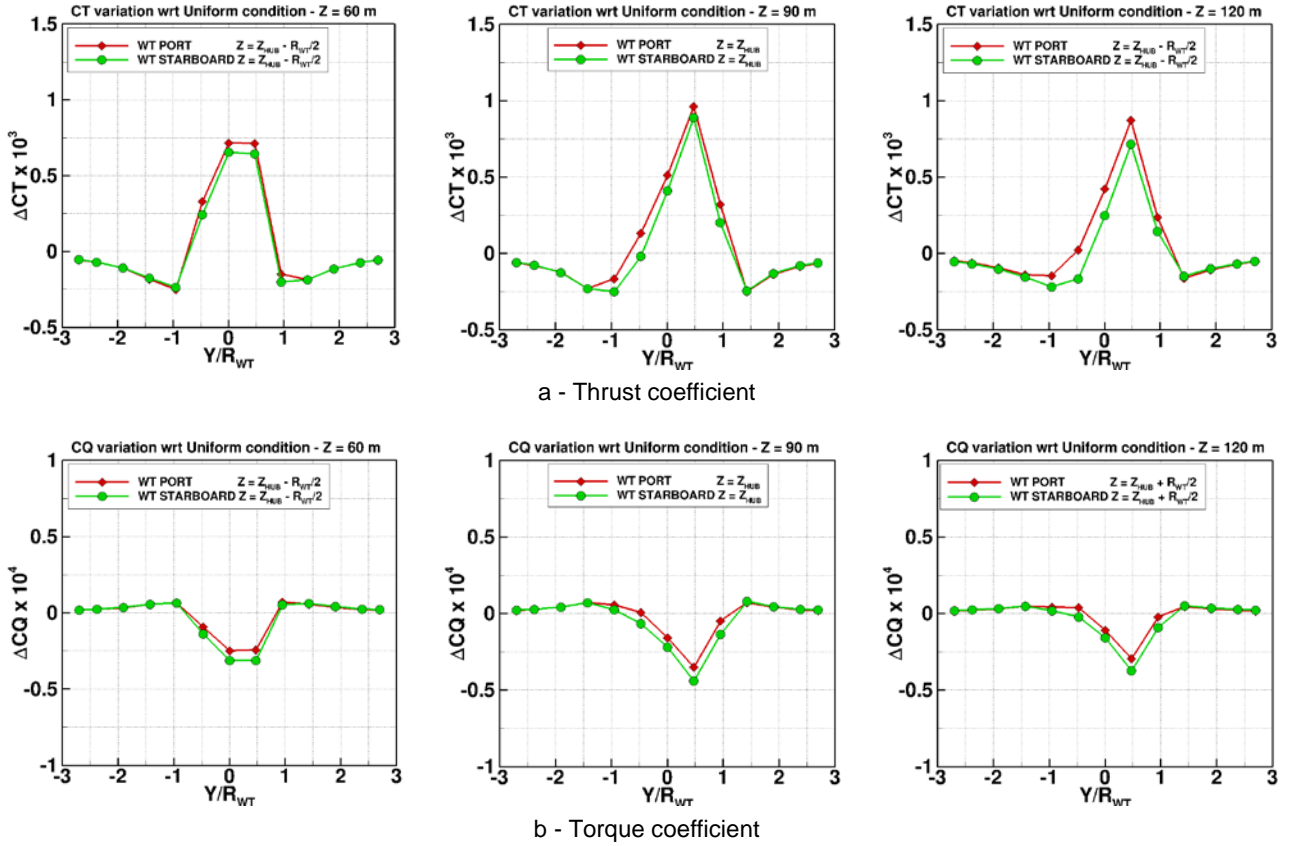


Figure 23: Variation of the rotor thrust coefficient (top) and bottom coefficient (bottom) with respect to the uniform conditions at the heights 60 m, 90 m, 120 m respectively. Helicopter leaving the WT disk on its port side R2L (red) or starboard side L2R (green) while crossing the WT wake

7 HANDLING QUALITIES INVESTIGATIONS

This section analyses the ADS-33 pitch and roll attitude quickness criterion^[11] in order to determine the sufficiency of attitude control margin when a helicopter is approaching the WT wake. To characterise the moderate-amplitude attitude change manoeuvres (i.e. $5^\circ < \theta < 30^\circ$, $5^\circ < \phi < 60^\circ$) ADS-33 introduces the so-called *pitch(roll) attitude quickness parameters*. This parameter from ADS-33 is defined as the ratio of the maximum pitch (roll) rate to the peak pitch (roll) attitude angle change, that is:

$$Q_\theta = \frac{q_{pk}}{\Delta\theta_{pk}} \text{ (sec}^{-1}\text{)}$$

$$Q_f = \frac{p_{pk}}{\Delta f_{pk}} \text{ (sec}^{-1}\text{)}$$

ADS-33 defines handling qualities boundaries for these parameters as a function of the minimum pitch (roll) attitude change $\Delta\theta_{min}$ ($\Delta\phi_{min}$) in the so-called pitch (roll) attitude-quickness criterion.

Figure 24 illustrates the Level 1/2 boundary attitude quickness for a general mission task element (MTE) in the case of a pitch manoeuvre, while Figure 25 shows the Level 1/2/3 boundary attitude quickness for a general mission task element (MTE) in the case of a roll manoeuvre according to the ADS-33. An aircraft should possess at least the Level 1 performance standards for

the pilot to be able to fly moderately aggressive low speed manoeuvres precisely and with minimal compensation.

The two figures present the vortex-induced pitch and roll attitude quickness charts, respectively, for the Bo105 helicopter considered in this paper.

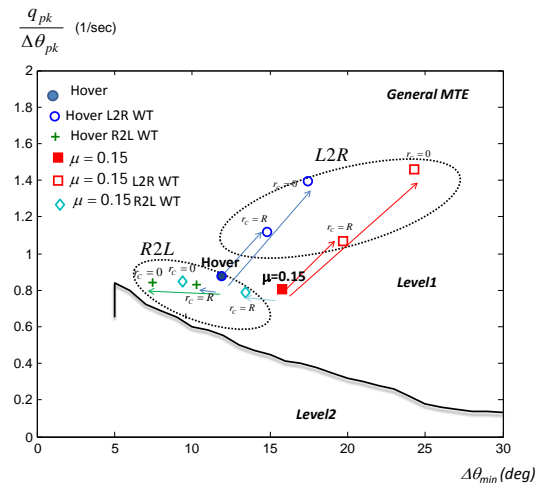


Figure 24: Pitch Attitude quickness charts for the helicopter encountering a WT wake.

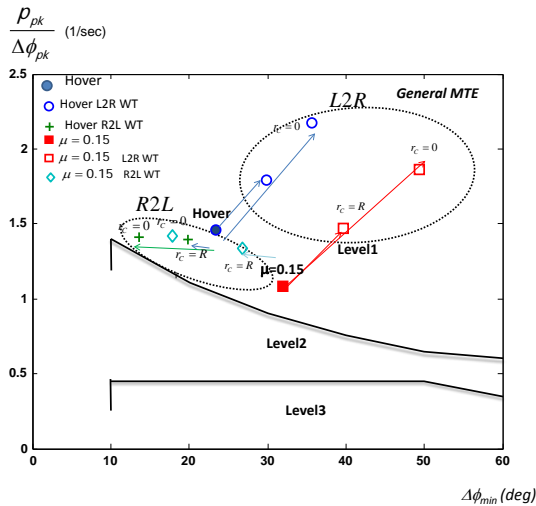


Figure 25: Roll Attitude quickness charts for the helicopter encountering a WT wake.

Two helicopter velocities are considered, hovering and an advance ratio $\mu=0.15$ with their pitch (roll) attitude quickness corresponding to Level 1 general MTE. From these initial conditions the helicopter is approaching the WT wake from L2R and R2L, the impinging position of the WT vortex being located, from the helicopter rotor centre, at a radial distance $r_c=0$ and $r_c=R$, respectively. Looking at the figure it can be observed that:

- For both pitch and roll attitude quicknesses in R2L helicopter position (vortex attacking the retreating side of the blade) result in moving to the left in the quickness charts. This will bring the helicopter closer to the Level 1/2 quickness boundary for general MTE and would give less adequate control for counteracting the effects of a vortex encounter;
- For both pitch and roll attitude quicknesses in L2R helicopter position (vortex attacking the advancing side of the blade) result in an increase in attitude quickness and much higher pitch(roll) changes especially when the vortex attacks at the helicopter hub centre. This would give less margin in control power terms for the helicopter to counteract the effects of a vortex encounter.
- Recalling the variation of the blade flapping angles with respect to the nominal conditions as illustrated in Figure 16, both the longitudinal and lateral flapping angles are increased when the side wind impinges the helicopter from L2R. This results in higher pitch (roll) rates for the helicopter and therefore in an increased pitch (roll) attitude quickness due to vortex-induced effects. This is because the attitude quickness parameter relates to agility, so momentarily there is more pitch (roll) rate that the pilot can command and therefore more pitch (roll) attitude quickness. It should be recognized that this situation is transient in nature and the pilot needs to command it only momentarily.

8 CONCLUSIONS

In the framework of the GARTEUR HC/AG-23 action group, the partners have been involved in technical activities dealing with the operations of helicopters immersed in the wake structures of large WTs. In particular, CIRA and the Delft University of Technology have investigated, from the aerodynamic and handling qualities point of view, the problem of a Bo105 helicopter rotor crossing, in low-speed level flight and in the presence of ABL, the wake of an NREL 5MW WT.

The selected crossing flight path has been assumed orthogonal to the WT axis and located two WT rotor diameters downstream to the WT disk. Three different flight altitudes have been investigated: above the WT hub; at the WT hub height; below the WT hub. Two flight directions have been simulated: R2L, with the helicopter leaving the WT disk on its port side; L2R, with the helicopter leaving the WT disk on its starboard side.

The aerodynamic simulations have been carried out by using a BEM methodology and applying a decoupled interactional procedure specifically conceived for the purpose. The rotor blades have been assumed fully rigid.

The simulations have been aimed at the understanding of the mechanism with which an interaction with a uniform side wind or WT wake can produce changes in the forces and moments acting on the helicopter rotor, and at their quantification.

The outcomes of the aerodynamic investigation are summarized in the following:

- despite the interactions produce complex flow fields, the phenomenology is substantially simple. A uniform side wind or a WT wake encountering a helicopter rotor locally alters the velocities acting on the helicopter rotor blades, in magnitude and/or direction, because of the WT axial and radial changes in velocity deficit; the presence of the WT blade tip vortices; the presence of the ABL; the WT wake swirl. These velocities modify the helicopter rotor blade sectional effective angles of attack, which, in turn, change the blade loads, generate flapping angles and alter the rotor forces and moments;
- an increase in the longitudinal flapping produces negative pitching moments (nose-down), while an increase in the lateral flapping causes positive rolling moments (port side-down);

In the particular case of uniform side wind, the comparison with the performance in undisturbed atmosphere has produced the following results:

- the flight direction R2L produces a reduction of the flapping angles, whereas the L2R one increases them. In both cases, this variation is significant for the cyclic angles, less important for the conicity. The amount of changes in the rolling and pitching moments are consequential. The yaw is little affected;
- the thrust and torque both increase during the flight in L2R direction. The opposite happens during the flight in R2L direction, but with lower intensity;
- the flight altitude has a negligible effect.

Regarding the interaction with the WT wake, the results have been compared with those in uniform side wind conditions. The following outcomes have been obtained:

- the flight altitude produces moderate changes;
- the effects on the flapping angles, loads and moments become important inside the WT wake, with peaks generally located around the WT hub position;
- the conicity slightly increases of about the same amount for the two flight directions;
- regarding the longitudinal flapping, the flight direction L2R produces a significant reduction of it. Instead, the flight direction R2L produces fluctuations of smaller amplitude. The effect on the pitching moment is direct: a significant rotor nose-up can be observed during L2R flight;
- the flight direction R2L produces an increase in the lateral flapping, whereas the flight direction L2R produces some fluctuations. The effect on the rolling moment is direct: a positive roll (port side-down) can be observed during R2L flight;
- the yawing moment slightly increases inside the wake with a maximum around the WT hub position. No difference can be observed by changing the direction of flight;
- the thrust increases significantly, while the torque reduces, independently of the flight direction.

Regarding the pitch and roll attitude quickness of the helicopter interaction with the WT wake, the following outcomes have been obtained:

- both pitch and roll attitude quickness in helicopter R2L flight brings the helicopter closer to the Level 1/2 quickness boundary for general MTE and would give wholly inadequate control for counteracting the effects of a vortex encounter;
- both pitch and roll attitude quickness in helicopter L2R flight results in an increased attitude quickness and much higher pitch changes especially when the vortex attacks at the helicopter hub centre. This would give less margin in control power terms for the helicopter to counteract the effects of a vortex encounter.

The analysis of the results has indicated that, for a WT rotor and helicopter rotor both counter-clockwise rotating, a pilot experiences a greater workload during the L2R flight. However, it should be recognized that this situation is transient in nature and the pilot needs to command it only momentarily.

9 REFERENCES

- [1.] <http://gwec.net/>;
- [2.] Wang, Y., White, M., Barakos, G.N., Wheeler, S., Tormey, P., Pantazopoulou, P., "Wind Turbine Wake Encounter by Light Aircraft," 40th European Rotorcraft Forum, Southampton, UK, Sep. 2-5, 2014;
- [3.] van der Wall, B. G., Fischenberg, D., Lehmann, P. H., and van der Wall, L. B., "Impact of Wind Energy Rotor Wakes on Fixed-Wing Aircraft and Helicopters," 42nd European Rotorcraft Forum, Lille, France, Sep. 5–8, 2016;
- [4.] van der Wall, B., Lehmann, P., "About the impact of wind turbine blade tip vortices on helicopter rotor trim and rotor blade motion," CEAS Aeronautical Journal, Vol.9, Nr.1, Mar. 2018;
- [5.] van der Wall, B. G., van der Wall, L. B., "Analytical Estimate of Rotor Controls Required for a Straight Vortex Disturbance Rejection – Technical Note," Journal of the American Helicopter Society, Vol. 62, Nr. 1, Jan. 2017;
- [6.] Bakker, R., and AG23 partners, "Wind Turbine Wakes and Helicopter Operations – Terms of Reference for the GARTEUR Action Group HC/AG-23," Feb. 2014;
- [7.] Visingardi, A., D'Alascio, A., Pagano, A., Renzoni, P., "Validation of CIRA's Rotorcraft Aerodynamic Modelling SYSTEM with DNW Experimental Data," 22nd European Rotorcraft Forum, Brighton, UK, Sept. 1996;
- [8.] Jonkman, J., Butterfield, S., Musial, W., Scott, G., "Definition of a 5-MW Reference Wind Turbine for Off-shore System Development," Technical Report NREL/TP-500-38060, Feb. 2009;
- [9.] Lehmann, P., "Bo105: Configuration Data," GARTEUR AG23 document, 2015;
- [10.] Spletstoesser, W.R., Junker, B., Schultz, K.-J., Wagner, W., Weitmeier, W., Protopsaltis, A., Fertis, D., "The HELINOISE Aeroacoustic Rotor Test in the DNW – Test Documentation and Representative Results," DLR-Mitt. 93-09, Dec. 1993;
- [11.] Anon., "Handling Qualities Requirements for Military Rotorcraft, Aeronautical Design Standard ADS-33E-PRF, Performance Specification," US Army AMCOM, Redstone, Alabama, March 21, 2000